Effect of Mg-doping ZnO nanoparticles on detection of low ethanol concentrations

S. Jaballah [a], M. Benamara [a], H. Dahman [a,*], A. Ly [b], D. Lahem [b], M. Debliquy [c], L. El Mir [a]

[a] Laboratory of Physics of Materials and Nanomaterials Applied at Environment (LaPhyMNE), Faculty of Sciences in Gabes, Gabes University, 6072, Gabes, Tunisia
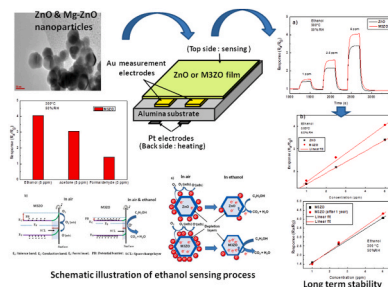[b] Materia Nova, Materials R&D Centre, Parc Initialis, Avenue Nicolas Copernic 1, 7000, Mons, Belgium
[c] Service de Science des Matériaux, Université de Mons, Rue de l'Epargne 56, 7000, Mons, Belgium

HIGHLIGHTS

- Pure and Mg (3 at.%) doped ZnO nanoparticles have been synthesized using sol–gel technique.
- The TEM observation shows prismatic shape and nanosized particles confirming the XRD results.
- 3 at% Mg doped ZnO (M3ZO) based gas sensor exhibits high sensitivity and excellent response to ethanol.
- M3ZO has highest Response/ppm ratio compared to literature results at 300 °C and 50%RH.
- M3ZO sensor Response exhibits, good linear relationship with concentration, and excellent long term stability.

GRAPHICAL ABSTRACT

Schematic illustration of ethanol sensing process

ARTICLE INFO

ABSTRACT

Pure and Mg-doped ZnO (3 at. %) nanoparticles were prepared based to sol–gel route under supercritical conditions of ethyl alcohol. The samples were characterized by certain techniques. XRD patterns showed the hexagonal wurtzite crystalline structure of ZnO and Mg-doped ZnO nanoparticles. The TEM image demonstrates the hexagonal shape and the nanometric size of the nanostructures. SEM images show the presence of hexagonal like shape nanoparticles and the increase of grain size for the Mg doped sample. The corresponding EDX analysis proves the existence of Mg with low concentrations and shows coherent distribution of high concentrations of Zn and O elements. The UV–Vis–NIR spectroscopy exhibits high absorbance of the prepared samples in the UV range. Thereafter, the effect of doping ZnO by Mg on sensing properties has been investigated. The obtained results outline an enhancement in sensing performances for Mg doped ZnO based sensor, which exhibits, competitive response and recovery times, high and linear response at working temperature 300 °C toward low and high ethanol concentrations with detection limit less than 1 ppm. Long term stability has been also investigated and sensor exhibits after one year, similar and reproducible responses.
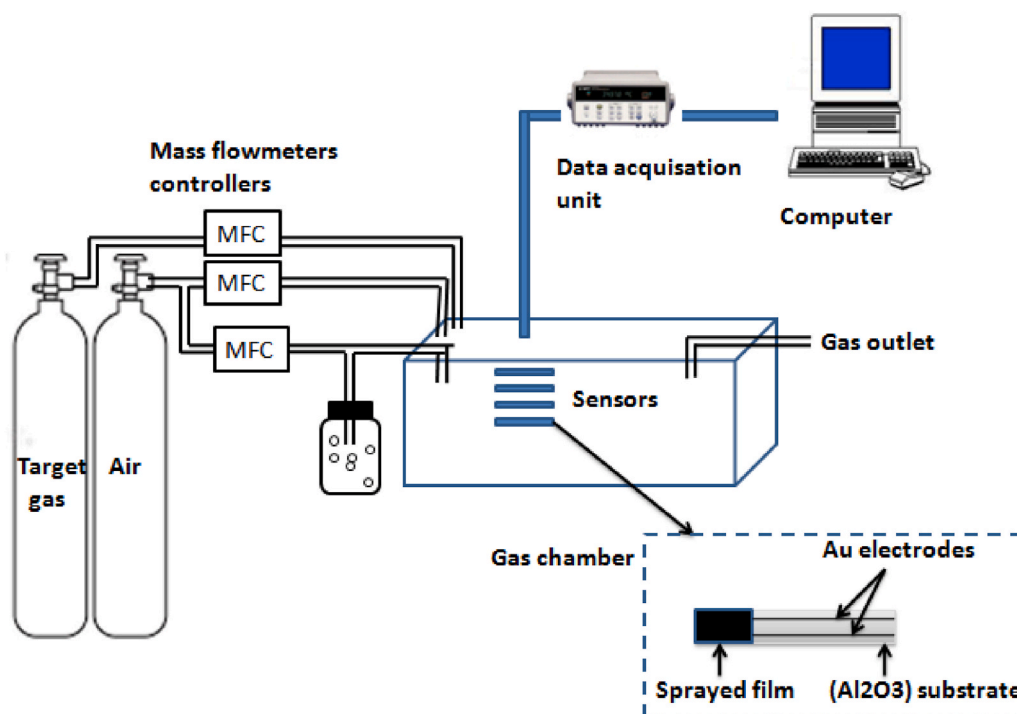
Fig. 1. Scheme of the experimental setup for gas sensors characterization.
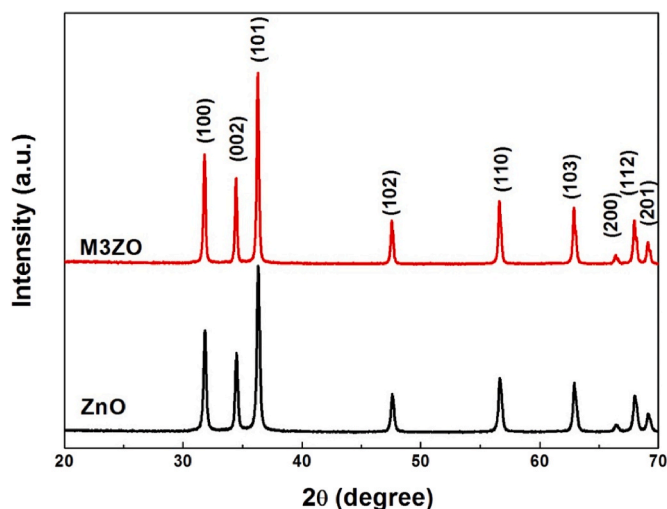

Fig. 2. X-ray diffraction patterns of the ZnO and M3ZO samples.
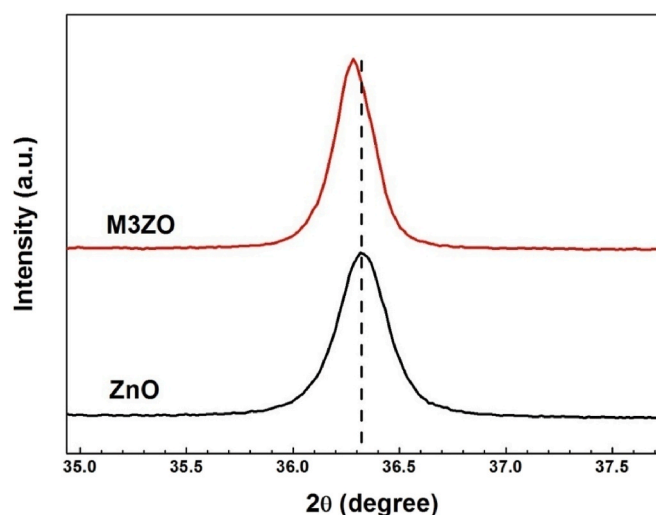

Fig. 3. Magnification of the (101) peak.

1. Introduction

With the rapid population growth, industrialization and emission of toxic gases, air pollution becomes more serious than ever and turns into a conspicuous risk to the environments in the biosphere. In order to protect environment and human health from air pollution, it is compulsory to monitor and detect toxic and poisonous chemicals in an effective way. Recently, researchers are trying to develop diverse types of chemical sensors such as potentiometric [1], amperometric [2], fiber optics [3], and biological sensors [4]. In latest years, metal oxide gas sensor (MOS) has also greatly drawn people's attention. Semiconducting metal oxides like ZnO [5], SnO_2 [6], NiO [7] and WO_3 [8] are widely used thanks to their advanced properties, chemical and time stability, low cost, and their capacity to detect hazardous gas like NO [9], NO_2 [10], LPG [11], NH_3 [12], CO [13,14], CO_2 [15] and ethanol [16].

Table 1
The 2θ, FWHM, lattices parameters (a,c), crystallites size (D), strain (ε) and gap energy (Eg) values for ZnO and M3ZO nanoparticles.

Sample	2θ (°) (101)	FWHM (101) peak (°)	a (Å)	c (Å)	D (nm)	ε (10^{-4})	Eg (eV)
ZnO	36.326	0.22874	3.245	5.200	38	7.6	3.24
M3ZO	36.286	0.17896	3.250	5.205	49	1.0	3.26

Large excitonic binding energy (60 meV), wide band gap (3.37 eV), high surface area and mobility of its conductive electrons, chemical and thermal stability and also well-organized molecular structure, makes ZnO semiconductor a specific and prominent candidate for gas sensing applications [17–19]. A diversity of ZnO nanostructures have been
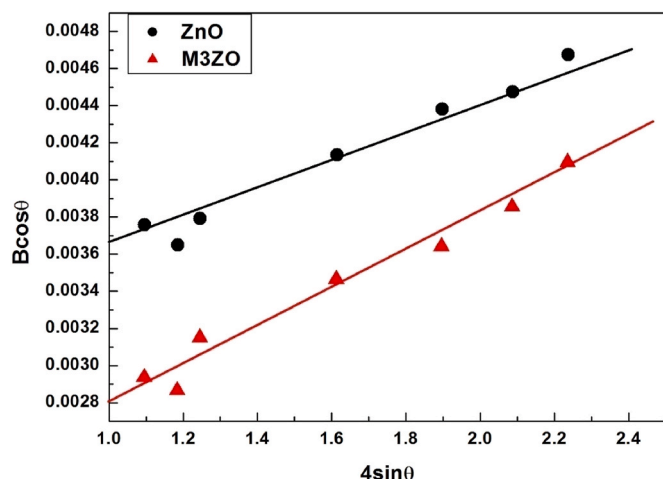
Fig. 4. Williamson-Hall's curves of ZnO and M3ZO samples.

utilized as sensing layers in gas sensors, including nanorods [20], films [21], nanoflakes [22], nanocomposites [23], nanoparticles [24] etc. Recently, Dang et al. [25] solvothermally synthesized ZnO nanorod with addition of nickel acetate tetra-hydrate (NA) and recorded high gas response and fast response/recovery times of sub-ppm level NO_2 (0.25–1.0 ppm) at operating temperature of 150–350 °C. Kanaparthi et al. [26] synthesized an ammonia (NH_3) sensor based on 2D ZnO nanoflakes with low detection limit (0.6 ppm). The sensor exhibited high sensitivity, reversible response and sub-15 s response and recovery times at an operating temperature of 250 °C. Similarly, Zhang et al. have elaborated Au/ZnO nanomaterials and have tested the sensing properties of 100 ppm of CH_4 at low temperatures [27].

Focusing on the properties of ZnO based gas sensor, the three S parameters (3S) including sensitivity, selectivity and stability are still not perfect. Some researches overcome this deficiency by adding suitable doping materials to ZnO lattice such as Al, Ca, Mg, Sn, Pd, etc … In recent work, we have showed that Ca dopant remarkably improves the sensing performances towards formaldehyde gas. The sensor showed, high response at about 5.28 (5 ppm, 250 °C) and very low detection limit (<1 ppm) [28]. Moreover, Aydin et al. [18] reported that Al improves the gas detection properties; Al-doped ZnO thin films based sensor have faster response time, better reversibility, more stable structure and higher response than pure ZnO. Also, Hjiri et al. [29] have prepared In-doped ZnO nanoparticles by sol–gel route and have investigated their sensing response toward CO gas which is improved compared to pure

ZnO. Besides, Mg doping was widely investigated thanks to its controllable band gap, less lattice mismatch with ZnO and good crystallinity [30,31]. That is why Mg doped ZnO is used as sensing layer in the domain of metal oxide gas sensors. Amin et al. have observed that doping ZnO with magnesium enhances the optical band gap and the sensing properties towards CO gas [32]. Khorramshahi et al. have fabricated highly oriented Mg doped ZnO thin film on Si(100)/SiO2 substrate using dip coated technique in temperature between 150 and 400 °C. Then they used it as active layer to detect Acetic acid vapor and it shows high sensitivity and fast response/recovery time [31]. Kulandaisamy et al. have also mentioned that Mg doped ZnO thin film based sensor exhibits a maximum response of 796 towards 100 ppm of ammonia at room temperature [33].

In this work, we concentrated to Mg doped ZnO nanoparticles elaborated by sol-gel method. We investigated their structural, morphological and optical properties and their gas sensing performances towards low ethanol concentrations. One of the novelties is that magnesium was used as doping element for the first time using our protocol. In several previous works, our lab's team has synthesized ZnO doped nanoparticles by the same modified sol-gel method. They have used a variety of doping like transition metals and IIA and IIIA elements. These doping materials have been used in a variety of applications e.g. photoelectric and photocatalysis devices, non enzymatic glucose biosensors and gas sensors. We have noticed that 3% level seems to be the
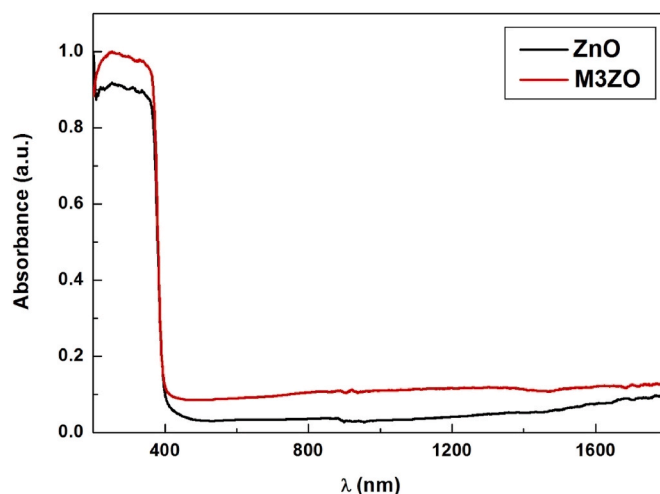

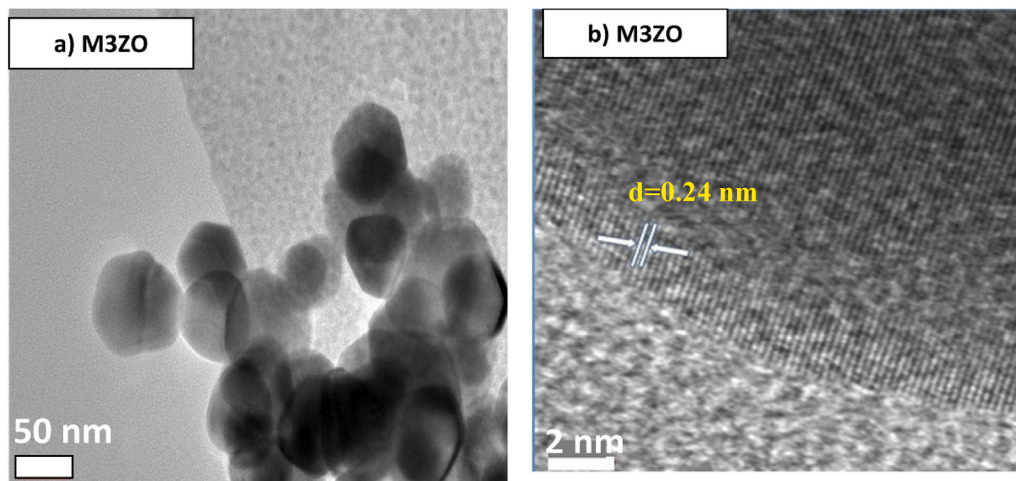**Fig. 6.** Absorbance spectra of pure and Mg doped ZnO nanoparticles.

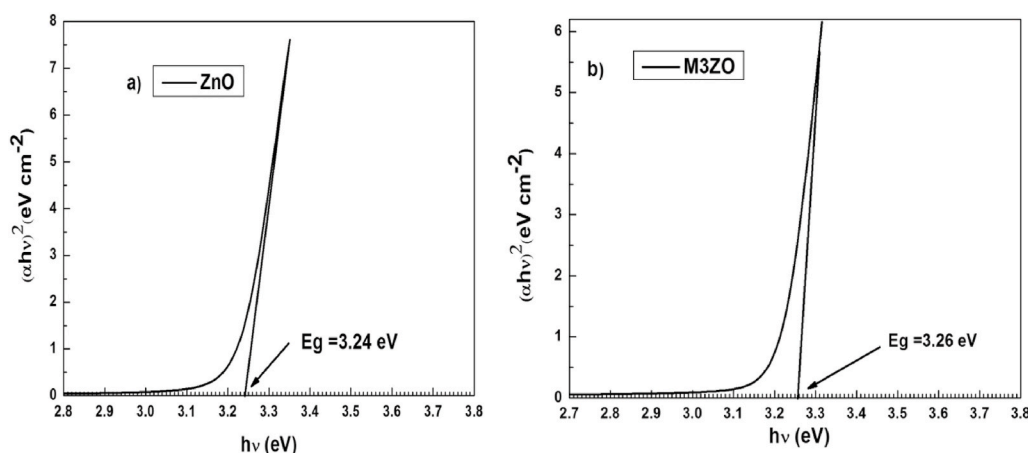**Fig. 5.** TEM images of M3ZO nanopowder at scale (a) 100 nm and (b) 2 nm.

Fig. 7. Plots of $(\alpha h\nu)^2$ vs. photon energy $h\nu$ of ZnO and M3ZO samples.
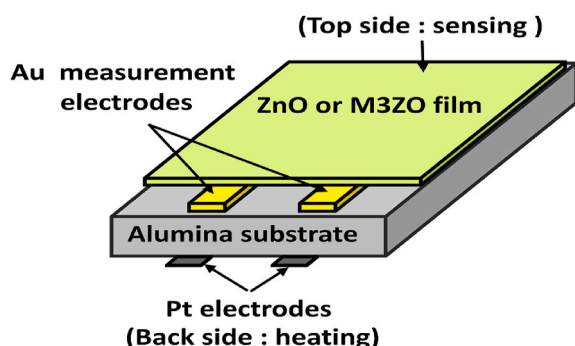

Fig. 8. Sensor architecture showing pre-deposited Au, Pt electrodes and deposited sensing film.

best concentration in majority of works [14,23,34–39]. In this context we have choose this concentration and in future work we will try to use others percentage of doping.

The measurements of ethanol play an important role in various fields, e.g food and microbiological industries, forensic science, clinical studies, environmental analyses, chemical and manufacturing industries [40,41]. Long-term ethanol misuse has several dangerous effects. It may cause nervous system damage, cancer, stroke, liver cirrhosis, cardiovascular diseases as well as psychiatric problems like anxiety, depression and personality disorder. On other hand, Alcohol consumption strongly affects the driving capability and increase car crash risk. Consequently, many countries define the threshold values blood alcohol concentration (BAC) for drivers [42]. The ethanol breath test will help the law to apply the punishment on the drunk driver [43].Therefore, researchers have a growing interest to the necessity of developing efficient gas sensor for the rapid and accurate detection of ethanol vapor because it is closely related to the issues of public health and safety [44]. Finally, the main challenge is the early detection and monitoring of ethanol at very low concentrations. In this context, Arakawa et al. [45] have constructed a highly sensitive biochemical gas sensor (bio-sniffer) for determining the concentration of ethanol on human skin. They carried out a selective measurement of ethanol gas in a concentration range of 25 ppb–128 ppm. On other hand, Liu et al. [46] have fabricated a promising gas sensor based on ZnO/SnO_2 composite for ethanol detection within the concentration range of 500 ppb–100 ppm. It showed excellent gas sensing properties at 225 °C.

ZnO doped Mg nanostructures have been widely used in different fields. In the gas sensor field, it shows sensitivity to multiple gases like CO [32], CH_4 [47] and H_2 [48]… However, it has been used for the detection of ethanol only by Kwak et al. [49] They have developed

Mg-doped ZnO nanowires by MgO-seeded vapor-phase growth. The prepared sensors have significantly enhanced the sensitivity and selectivity to ethanol. However it seems that the signal needs long time to return to the initial baseline resistance (more than 800 s) that is to say for gas desorption. In our case, the sensors are prepared by an easier method which requires lower energy consumption and shows faster recovery times. Finally, in our knowledge, it is the first time that ZnO doped Mg in the form of nanoparticles has been used for ethanol detection.

2. Experimental process

2.1. Elaboration of Mg doped ZnO nanoparticles

A facile sol-gel route was used for the elaboration of ZnO nanoparticles. We dissolved 16 g of dehydrate zinc acetate (Zn $(CH_3COO)_2.2H_2O$, 99%) in 112 ml of methanol with magnetic stirring for 10 min. Then, the whole is introduced into 1L stainless steel autoclave with 220 ml of ethyl alcohol and we proceed to a drying at a temperature of 250 °C, slightly higher than the critical conditions of ethanol (Tc = 243 °C, Pc = 63.6 bars) in keeping with L. El Mir et al. protocol [50,51]. Then, the resulting powders are heat-treated in air in a muffle furnace at about 2 h at 400 °C. For the preparation of Mg doped ZnO nanoparticles, we added to the previous solution an adequate amount of $MgCl_2.6H_2O$ as Mg precursor, according to atomic ratio of 0.03 before proceeding to drying step. In the following, the synthesized nanopowders will be tagged as ZnO and M3ZO in accord to nominal doping content.

2.2. Characterization

The structural characterization was executed using X-ray diffraction device named Philips PW1710. The morphological characterization of the prepared samples were performed using scanning electron microscope (SEM) equipped with EDX (FE-SEM, S4800II, Hitachi, Japan). Also, the morphological properties are investigated by a transmission electron microscopy (TEM). The TEM was executed with a JEOL JEM 2010 electron microscope (LaB6 electron gun) using an accelerating voltage of 200 kV equipped with Gatan 794 Multi-Scan CCD camera for digital imaging. The optical measurements were investigated in the UV–Vis–NIR regions, in the wavelength between 200 and 1800 nm, using Shimadzu UV-3101PC spectrophotometer equipped by integrated sphere.

For sensing tests, we put 250 mg of M3ZO nanopowders in 2.25 ml of distilled water. Then we have sonicated the mixture during 15 min by an ultrasonic until obtained uniform dispersion. Thereafter, we deposited the solution using a spray method on alumina substrates (Al_2O_3) (C-MAC
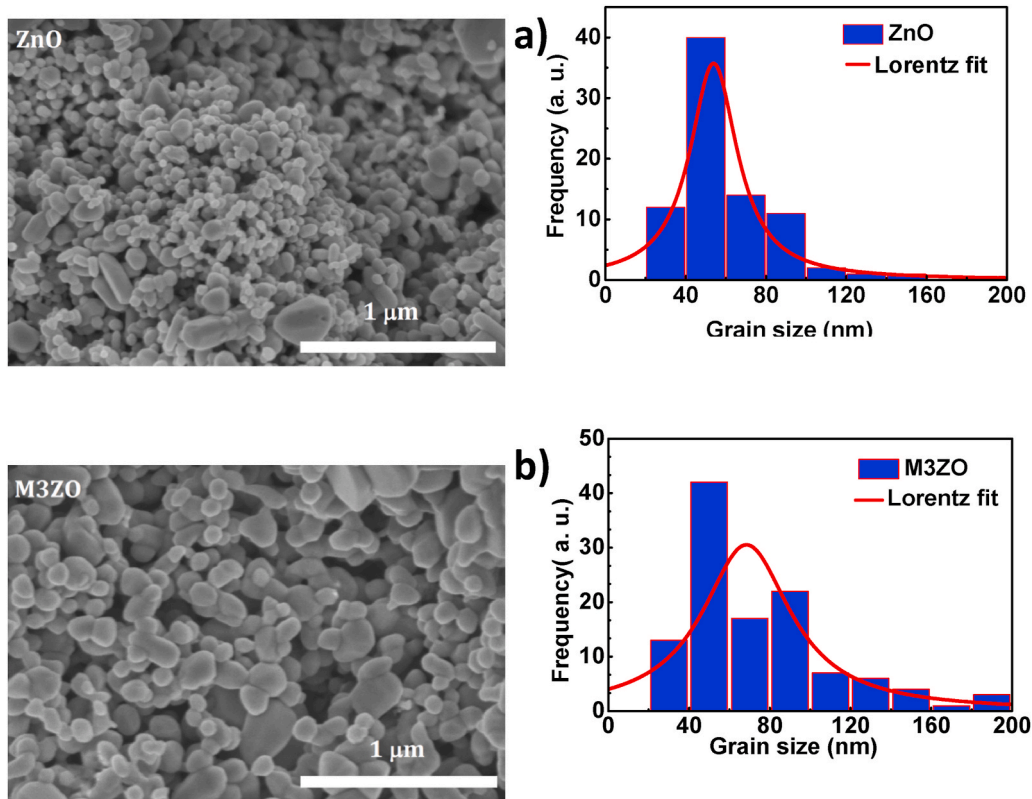
Fig. 9. SEM images and grain sizes distribution of (a) ZnO and (b) M3ZO sprayed films.

Micro Technology Company, Belgium) equipped with a pair of inter-digitated gold electrodes and back-side Pt heating elements. With a view to stabilize the deposited film before sensing tests, the sensor was heated during 1h at 400 °C. The sensing tests are realized in a home-made gas sensing measuring system. The experimental platform was composed of gas sources, mass flowmeters controllers (MFC, Bronkhorst High-Tech, Netherlands), testing chamber, computer and controlled data acquisition, as presented in Fig. 1. At first, the prepared sensors were placed in a testing chamber made of stainless steel with an inside surface of Teflon. Then, commercial synthetic air (79% N2+21% O2) was injected into the chamber until baseline stabilization. After that, we inject the target gas with suitable concentrations. The humidity level of gas was controlled by mixing dry and wet air by bubbling in deionized water at 25 °C. Relative humidity (RH) and temperature were continuously monitored. More details may be getting it in the following references [52–55]. The gas sensor response is specified as S= Ra/Rg where Ra and Rg represent the sensor's resistance in air and under target gas respectively.

3. Results and discussion

Fig. 2 reports the XRD patterns of ZnO and M3ZO nanoparticles. Nine diffraction peaks are pronounced, showing the polycrystalline structure of the synthesized samples.

The peaks are assigned to the (100), (002), (101), (102), (110), (103), (200), (112), and (201) plans. These observed diffraction peaks are consistent with the ZnO hexagonal wurtzite structure and matched well with the standard JCPDS data NO. 36–1451 [56]. No additional diffraction peaks related to Mg are observed. This may be attributed to the low Mg content.

As can be shown in Fig. 3, the Mg doping leads to an increase in the intensity and sharpness of the (101) diffraction peak.The full width at half maximum (FWHM) of the (101) peaks decreased for the M3ZO samples (as mentioned in Table.1). Thus, the crystallinity of M3ZO naoparticles was improved. Moreover, a little shift of the ZnO (101)

diffraction peak towards the lower 2-theta degrees is noted for Mg doped ZnO sample. This shift proves the incorporation of Mg ion into the ZnO lattice. Besides, this deviation is may be attributed to the increase of micro-strain involved by the small difference between the ionic radii of the Mg^{2+} and Zn^{2+} [56]. Eqs. (1) and (2) gives access to the lattice constants a and c. The calculated values are given in Table1.

$$\frac{1}{d^2} = \frac{4}{3a^2}\left(h^2 + k^2 + hk\right) + \left(\frac{l^2}{c^2}\right) \qquad (1)$$

$$2d_{hkl}\, sin\theta = n\lambda \qquad (2)$$

where d is the inter-reticular distance, a, c are the lattice parameters of the ZnO wurtzite hexagonal structure, (h, k, l) are the Miller indices, θ is the Bragg diffraction angle and λ = 1.541874 Å is the X-ray wavelength. These obtained values of ZnO nanoparticles are in good agreement with the literature ones [57] and show small increase for the M3ZO sample. Lattice expansion is probably related to lattice strain [58].

The average crystallite size, D, and the strain ε have been assessed from the Williamson-Hall equation (Eq. (3)) [59].

$$\beta_{hkl} \cos\theta = \frac{K\lambda}{D} + 4\varepsilon \sin\theta \qquad (3)$$

where β means the full width at half maximum (FWHM) of the XRD peak, K is the shape factor (0.9). The different estimated values are illustrated in Table 1. Based on βcosθ versus 4sinθ plot (Fig. 4), the lattice strain and crystallite size are obtained from the slope and the intercept Kλ/D respectively. The calculated strain was increased from 0.0007 to 0.001 with Mg substitution. Besides, the average crystallites size was 38 and 49 nm for ZnO and M3ZO samples respectively.

The increase of crystalline size shows that Mg doping may enhance the grain growth. This increase may be due to a nucleation phenomenon [60].

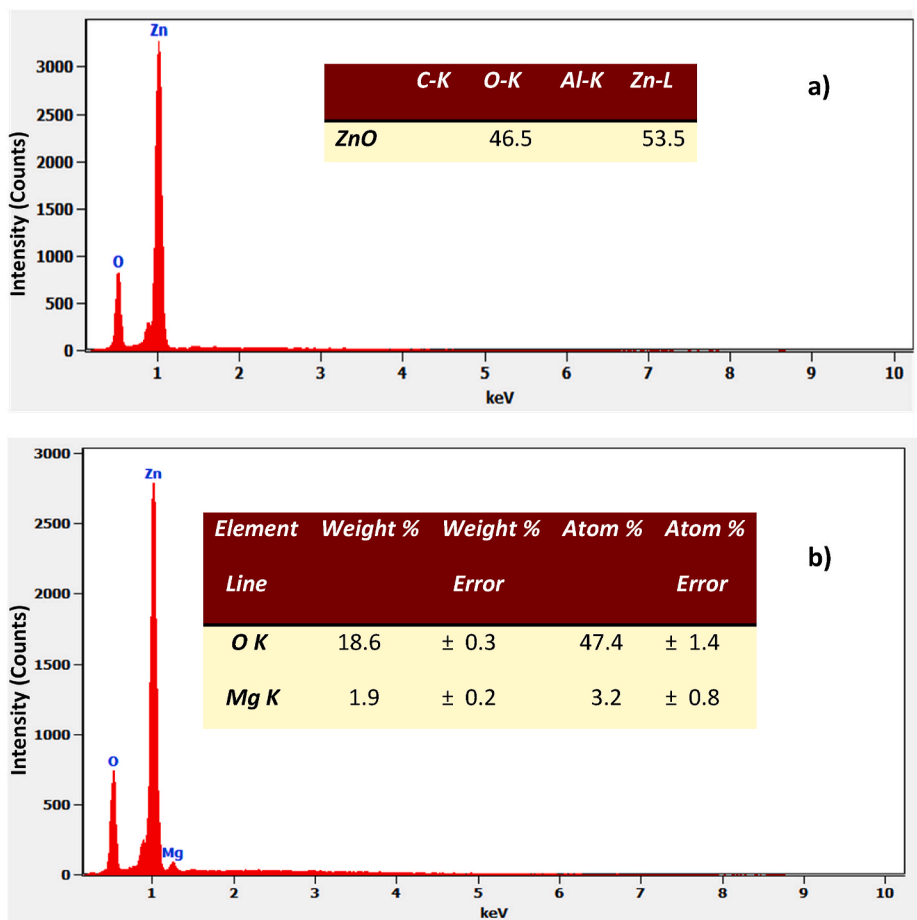Fig. 5 a) shows TEM images of M3ZO nanoparticles. Very small

	C-K	O-K	Al-K	Zn-L
ZnO		46.5		53.5

Element Line	Weight %	Weight % Error	Atom %	Atom % Error
O K	18.6	± 0.3	47.4	± 1.4
Mg K	1.9	± 0.2	3.2	± 0.8

Fig. 10. EDX spectra of a) ZnO and b) M3ZO nanoparticles.
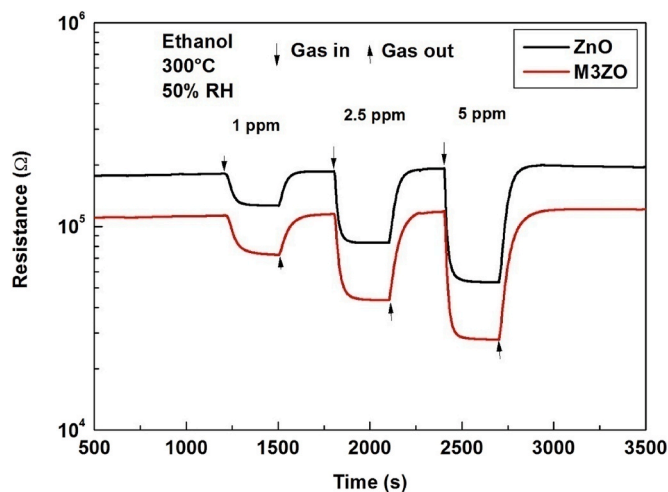

Fig. 11. Dynamic resistance change of ZnO and M3ZO based sensors towards ethanol at operating temperature of 300 °C and 50% RH.

particles in the range of nanometer are observed and described by the presence of crystallites having a hexagonal shape. The crystallites size varies between 40 and 60 nm. The average crystallite sizes are in accordance with that calculated from Williamson-Hall relationship (49 nm). Fig. 5 b) shows HRTEM picture of M3ZO nanopowders and the measure lattice fringes were approximately 0.24 nm, which match up to the (101) plane of the hexagonal ZnO phase.

Fig. 6 depicts the UV–Vis–NIR absorption spectra for wavelengths between 200 and 1800 nm of undoped and Mg doped ZnO nanoparticles.
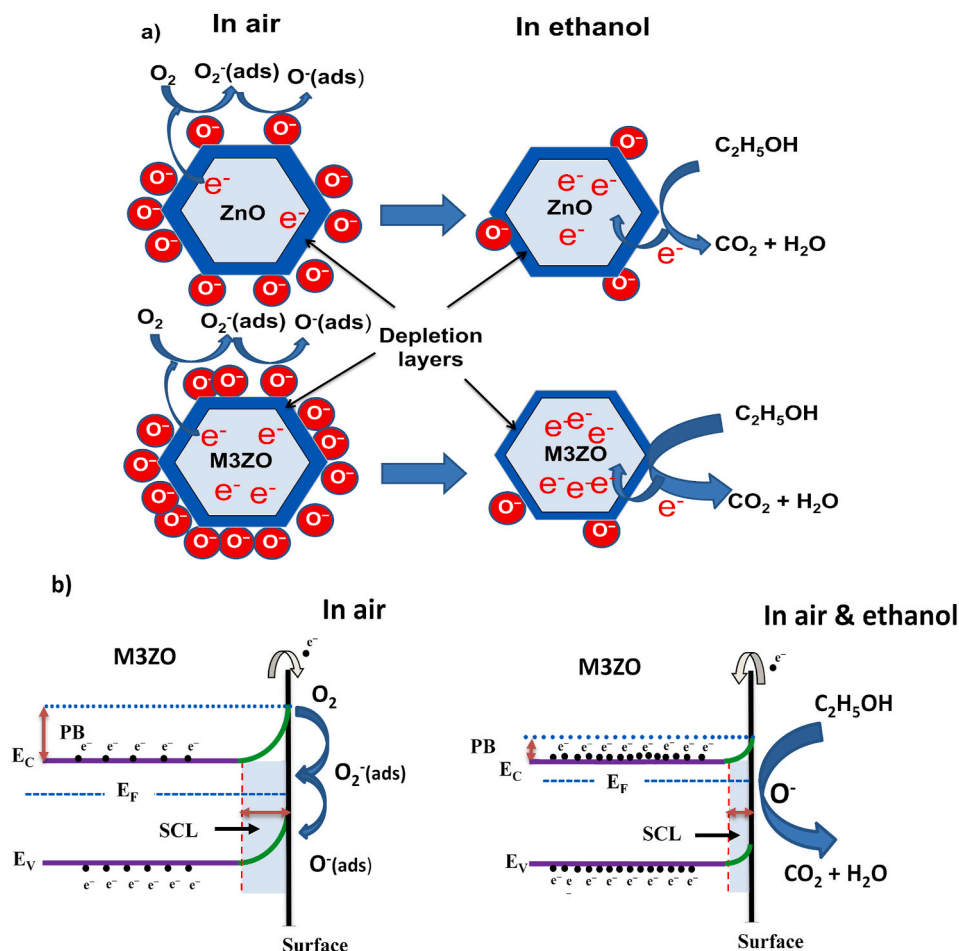
The absorption curves exhibit an intense absorption in the UV range. The absence of others absorption peaks showed the good optical properties of the samples. Adding Mg modifies the absorption characteristics of nanostructures. Indeed, the intensity of the absorbance band at the UV region increases for M3ZO nanoparticles, which is possibly a result of the increase of free carriers concentration that may absorb light [61]. The gas tests results below indicate that the Mg doped ZnO presents higher conductivity that pristine ZnO. This support the idea of increase of the concentration of the free charge carriers. The band gap energy, for a direct gap semiconductor is estimated from the absorption spectrum ($\alpha h\nu$) through Eq. (4):

$$(\alpha h\nu) = A\left(h\nu - E_g\right)^{\frac{1}{2}} \tag{4}$$

where α is the absorption coefficient, $h\nu$ presents the photon energy, E_g is the gap energy and A will be a constant.

The spectrums of $(\alpha h\nu)^2$ in terms of the photon energy ($h\nu$) for the synthesized samples are shown in Fig. 7. The optical gap energy (Eg) of each sample was gotten by extrapolating the linear part of the curve to the x-axis ($\alpha = 0$).

The estimated band gap values are 3.24 and 3.26 eV respectively for ZnO and M3ZO samples with incertitude of 0.01 eV. The band gap energy values are confirmed by using the Kubelka-Munk method. The optical band gap energy increases a little for M3ZO sample. Mg is responsible for the small enhancement of gap energy. The present increase in the gap energy is theoretically obtained by other research group [60]. Rouchdi et al. indicated that the broadening of band gap may be related to defects introduced into the ZnO lattice owing to the difference in electronegativity and ionic radius of Zn and Mg atoms.

E_V: Valence band; E_C: Conduction band; E_F: Fermi level; PB: Potential barrier; SCL: Space charge layer

Fig. 12. a) Schematic illustration of ethanol sensing process and b) energy band structure of M3ZO based sensor.
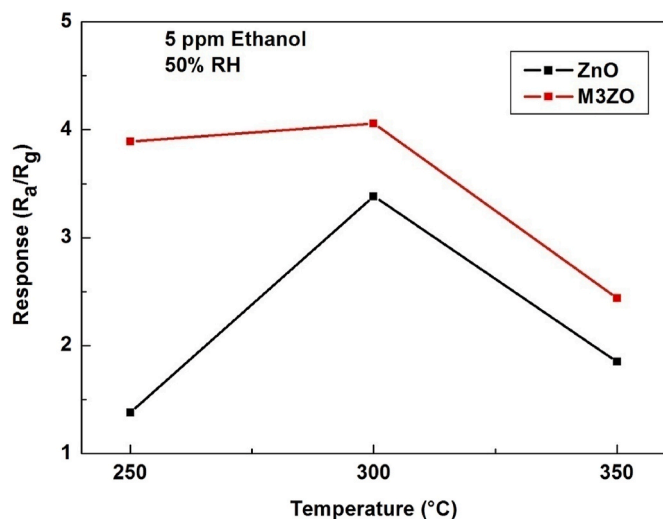

Fig. 13. Response versus operating temperatures at 50% RH of ZnO and M3ZO based sensors towards 5 ppm ethanol.

The obtained nanopowders were used to fabricate the sensing film of the sensor by spray technique. Fig. 8 shows the sensor architecture with sensing and heating electrodes and sensing film.

The SEM micrographs displayed in Fig. 9 illustrate the surface morphology and the aggregates size distribution of sprayed ZnO and M3ZO films. ZnO and M3ZO layers show hexagonal like shape nanoparticles with dispersion in size. By adding the magnesium, more dispersion and higher grain sizes may be observed as depicted in Fig. 9 a).

It can be proposed that the presence of magnesium, induces a raise of defects in the ZnO structure, enhances the grains' surface energy, and thus promotes their agglomeration.

EDX spectra shown in Fig. 10 are used in order to analyze the purity of the prepared samples as well as to prove the presence of constitutional elements.

The EDX spectrum of pure ZnO is composed of Zn and O elements with corresponding contents of 53.5% and 46.5%, respectively showing that our ZnO is under-stoichiometric. However, for M3ZO based sensor, the EDX spectra shows the presence of peaks related to Zn, O and Mg elements. Their corresponding contents are 49.5%, 47.4% and 3.2%, respectively. It is worthwhile noticing that no relevant percentage of any contaminant species was detected.

As shown in Fig. 11, the sensor resistance decreased during exposure to 1–5 ppm of ethanol, in accordance to the generally sensing mechanism on n-type oxide semiconductors. In fact, the gas detection mechanism is relied on a variation in electrical conductivity or resistance due to gas adsorption and desorption on the sensor's surface [62].

Depending on the temperature, the adsorbed oxygen molecules become O_2^- (<100 °C), O^- (100–300 °C), or O^{2-} (>300 °C) [63]. This provokes the formation of a depletion region on the surface leading to the increase of the resistance [64]. When the sensor is exposed to
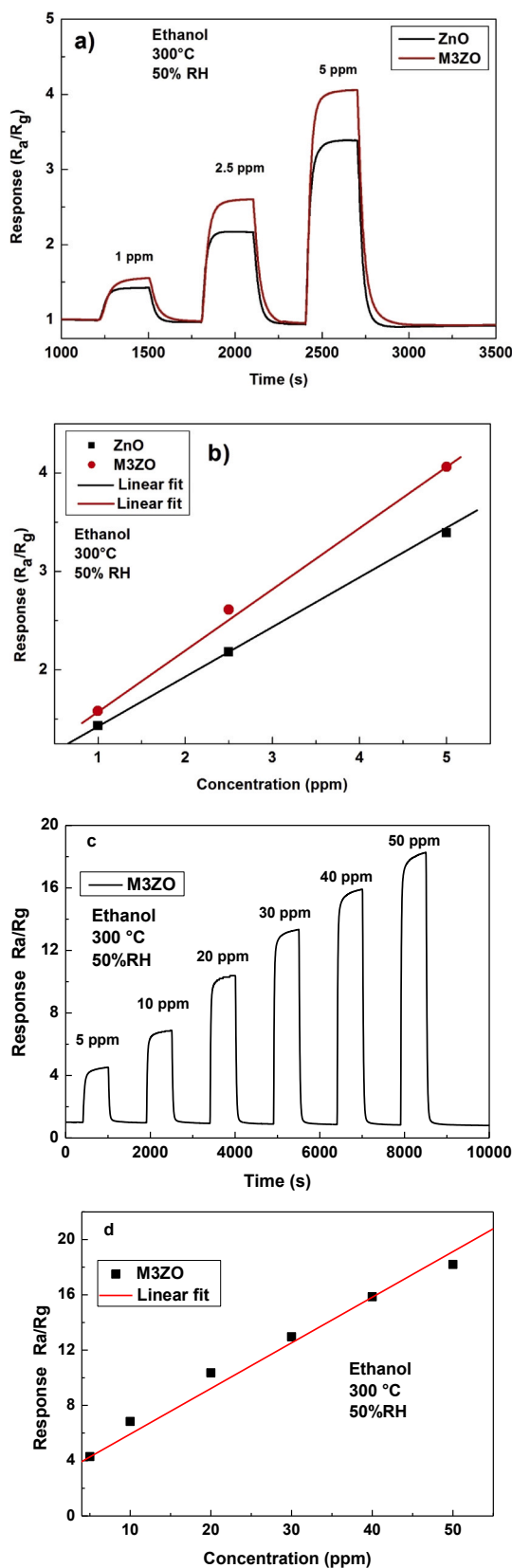
Fig. 14. a) Responses of ZnO and M3ZO based sensors to 1–5 ppm ethanol exposure at the working temperature of 300 °C and b) Calibration curves, c) Responses of M3ZO at higher concentrations (5–50 ppm) and d) calibration curve.
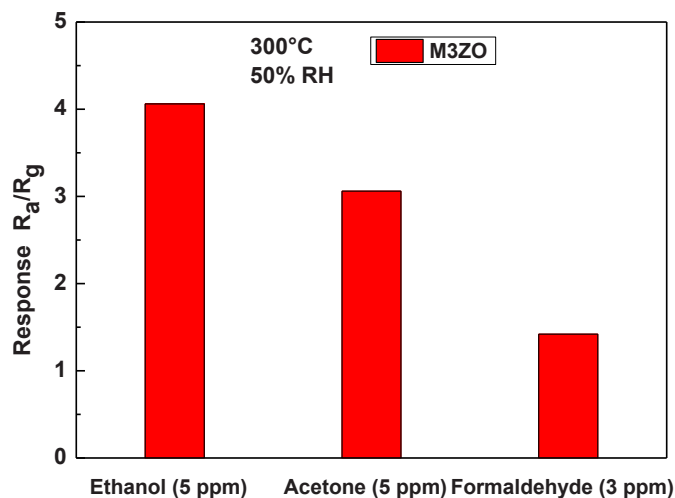

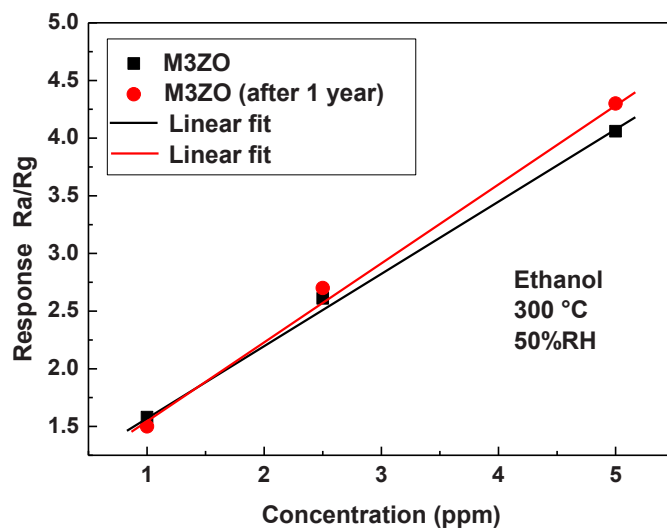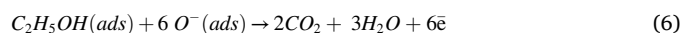**Fig. 15.** M3ZO sensor selectivity at 300 °C and 50% RH.

Fig. 16. Long term stability of M3ZO sensor.

ethanol, the adsorbed oxygen interacts with this injected gas and the trapped electrons are releasing back in the conduction band. Thus, the conductivity of the M3ZO nanoparticles increases. It can be supposed that the replacement of the Zn^{2+} cation by the Mg^{2+}, which acts as a donor, generates active adsorption sites which favor the adsorption of oxygen species. In this way, Mg^{2+} sites enhanced the reaction of ethanol with oxygen species. The global reaction of ethanol with ionic oxygen species is described by Eqs. (5) and (6) [65].

$$O_{2(ads)}^- + e^- \rightleftarrows 2O_{(ads)}^- \tag{5}$$

$$C_2H_5OH(ads) + 6\,O^-(ads) \rightarrow 2CO_2 + 3H_2O + 6\bar{e} \tag{6}$$

Moreover, Fig. 12 a) presents a schematic illustration of ethanol sensing mechanism for ZnO and M3ZO based sensors, however in Fig. 12 b), we illustrate, the bands diagrams, the Fermi level and the potential barrier for M3ZnO based sensor in air and under air and ethanol mixture atmosphere. When the sensor was exposed to ethanol, the space charge layer decreases leading to the increasing of the material conductivity and thus the decreasing of the sensor resistance.

Fig. 13 depicts the responses of ZnO and M3ZO sensors to 5 ppm ethanol as a function of the testing temperature ranging from 200 to 350 °C in humid air (50%RH).

Table 2
Comparison of ethanol sensing characteristics with literatures results.

Sensing material	Temperature (°C)	Ethanol (ppm)	Response	(Response/ppm) x100	Reference
Ga2O3–ZnO nanohybrids	300	300	120 #	40	[68]
Al-doped ZnO nanosheets	370	100	90.2*	90.2	[69]
Ag/ZnOnanorods	360	100	36.5*	36.6	[70]
Flower-liked Ce doped ZnO	300	100	72.6*	72.6	[71]
Na-dopedZnOnanorods	300	100	45	45	[72]
K-dopedZnOnanorods	300	100	45.2	45.2	[72]
Co-doped ZnO microspheres	220	5	3.3*	66	[73]
Mg doped ZnO	300	5	4*	80	**Our work**

(*) and (#) correspond respectively to $\dfrac{Rair}{Rgaz}$ and $\dfrac{Rair - Rgaz}{Rgaz}$.

We notice that the responses to ethanol for both sensors increase to a maximum value with the increasing temperature and subsequently decreased for further increase in temperature. The optimal working temperature for both sensors is determined to be 300 °C. The variation of response as a function of temperature is assigned to the chemisorptions and surface reaction [66]. In fact, by increasing the temperature up to 300 °C, the thermal energy is sufficient for the gas molecules to get over the activation energy barrier and interact with the oxygen species absorbed at the surface. Nevertheless, for a higher temperature, the amount of adsorbed oxygen species is lower which give rise to a decrease in the response. The M3ZO based sensor shows higher response toward 5 ppm ethanol than ZnO sensor. At 250 °C the response value is about 2.8 times higher than that of pure ZnO sensor.

Fig. 14 a) displays the responses of ZnO and M3ZO based sensors, as a function of time at the optimal working temperature 300 °C and 50% RH. It can be obviously seen that the M3ZO sensor has higher response as pure ZnO toward ethanol. Also M3ZO sensor response increases sharply and continuously with increasing of the ethanol concentration from 1 to 5 ppm, indicating that M3ZO sensor can be used as the promising material for ethanol sensor at low ethanol gas concentrations. As the calibration curve presented in Fig. 14 b) shows, the M3ZO sensor response exhibits good linear relationship with the concentration, which considered a great potential for practical applications. The responses of M3ZO sensor at higher concentrations (5–50 ppm) are also investigated and results are depicted in Fig. 14 c. The associated calibration curve is presented in Fig. 14 d witch confirms the linear trend.

Selectivity is one of the important parameter of gas sensor which signifies the ability of a sensor to respond to a particular gas in presence of other gases. With a view to study the selectivity of the M3ZO sensor toward ethanol, the sensor responses to 5 ppm acetone and 3 ppm formaldehyde at 300 °C are measured. The obtained results are shown in Fig. 15, from which we can see that, the response to ethanol is much higher than that recorded for other VOC's gases. Long term stability of M3ZO based sensor was also investigated. Calibration curve of M3ZO sensor to different ethanol concentrations at 300 °C over a period of 1 year is shown in Fig. 16. It's noticed that, after almost a year the sensor still responsive and it gives approximately the same responses if we consider calculation errors. The comparable response values indicate that the M3ZO sensor has good potential in actual field applications.

Based on previous studies, the improvement response of M3ZO sensor towards ethanol gas can be attributed to some factors like small-sized particle, higher surface roughness, stacking defects, amount of oxygen vacancies as well as band gap values [31,67]. XRD characterization depicts that particles sizes increases for M3ZO compared to ZnO nanoparticles. So, we cannot attribute the enhancement of gas sensor response to small-sized particles. However, the UV–Vis results show that M3ZO rise up slightly the energy band-gap as well as the intensity of the absorbance bands of ZnO which induce increase of charge carrier concentration. This increase of charge carrier can be viewed as one reason for the increase of gas response. Then, it seems that M3ZO based sensor displays excellent gas-sensing performances towards ethanol, including relatively low operating temperature, high response, and low detection limit.

The response of the sensor was compared to recently works with other ZnO doped nanostructures. Table.2 shows the comparison of gas-sensing properties between M3ZO nanoparticles and other sensing nanomaterials toward ethanol gas.

Cao et al. [69] have synthesized Al-doped ZnO ultrathin nanosheets based sensor which showed notable ethanol sensing properties. Although, they have found higher response, they used higher temperature at about 370 °C. As it showed, Wei et al. [70] have also used high working temperature at about 360 °C in order to detect 100 ppm ethanol. The reported response is at about 36.5 (lower than our M3ZO response). In fact, working temperature is one of the gas sensors performances that we are trying to decrease. Now, comparing to other cited examples, which use 300 °C [68,71,72], our M3ZO sensor, shows a remarkably higher sensitivity. Therefore, Xu et al. [73] synthesized hybrid Co-doped ZnO microspheres using solvothermal method. They tested these nanospheres for the detection of ethanol (5–100 ppm) and reported a relatively good response at 220 °C. Even, they used lower working temperature; our M3ZO shows higher response in 50% relative humidity, lower detection limit (≤1 ppm) and easier and faster synthesis method. Finally, considering the simple synthesis method and good gas sensing performances, M3ZO is a hopeful candidate for efficient and highly sensitive of ethanol detection.

4. Conclusion

During this work, pure and Mg (3 at.%) doped ZnO nanoparticles have been prepared by sol–gel technique. XRD investigation has shown that the structure of M3ZO nanoparticles was polycrystalline, and hexagonal wurtzite. The sizes of the crystallites were calculated by the Williamson-Hall's method and show an increase for M3ZO sample. The TEM observation shows prismatic shape and nanosized particles confirming the XRD results. The SEM images of sensors sprayed layers, show nanoparticles with hexagonal like shape and the EDX outlines the presence with good stoichiometry of Zn, O and Mg elements. Analyzes by UV–Vis–NIR spectroscopy indicated that the samples have a high absorbance in the UV range and the gap energies, calculated using Tauc plots, show small increase after doping. Sensing tests at working temperature 300 °C and 50%RH, outline linear response versus ethanol concentrations, for low and high concentrations and show that Mg incorporation may enhance sensor performances. Furthermore, the M3ZO based sensor exhibits long term stability, indeed after one year, the sensor shows similar performances. Schematic illustration of ethanol sensing process was exposed. The obtained M3ZO based sensor was found to be an inspiring sensing material and exhibits competitive response and recovery times and the highest response to concentration ratio at 300 °C working temperature, comparing to previous studies.

CRediT authorship contribution statement

S. Jaballah: Funding acquisition, Writing - original draft, substantial contribution to preparation, substantial contribution to acquisition of

data, drafting the article. **M. Benamara:** Funding acquisition, substantial contribution to acquisition of data. **H. Dahman:** Formal analysis, Data curation, Writing - original draft, substantial contribution to analysis and interpretation of data, drafting the article, final approval of the version to be published. **A. Ly:** Funding acquisition, substantial contribution to acquisition of data. **D. Lahem:** Formal analysis, Data curation, substantial contribution to analysis and interpretation of data, critically revising the article, final approval of the version to be published. **M. Debliquy:** Formal analysis, Data curation, Writing - review & editing, substantial contribution to analysis and interpretation of data, critically revising the article. **L.E.L. Mir:** Writing - review & editing, critically revising the article.

Declaration of competing interest

The authors declare that they have no known competing financial interests or personal relationships that could have appeared to influence the work reported in this paper.

Acknowledgements

References

[1] J.F. Baez, M. Compton, S. Chahrati, R. Cánovas, P. Blondeau, F.J. Andrade, Controlling the mixed potential of polyelectrolyte-coated platinum electrodes for the potentiometric detection of hydrogen peroxide, Anal. Chim. Acta 1097 (2020) 204–213, https://doi.org/10.1016/j.aca.2019.11.018.

[2] J. Lee, G. Hussain, N. López-Salas, D. MacFarlane, D.S. Silvester, Thin films of poly (vinylidene fluoride-co-hexafluoropropylene)-ionic liquid mixtures as amperometric gas sensing materials for oxygen and ammonia, Analyst 145 (5) (2020) 1915–1924, https://doi.org/10.1039/C9AN02153A.

[3] R. Kitture, D. Pawar, C.N. Rao, R.K. Choubey, S. Kale, Nanocomposite modified optical fiber: a room temperature, selective H2S gas sensor: studies using ZnO-PMMA, J. Alloys Compd. 695 (2017) 2091–2096, https://doi.org/10.1016/j.jallcom.2016.11.048.

[4] P.D. Howes, R. Chandrawati, M.M. Stevens, Colloidal nanoparticles as advanced biological sensors, Science 346 (2014) 1247390, https://doi.org/10.1126/science.1247390.

[5] M. Hjiri, R. Dhahri, K. Omri, L. El Mir, S.G. Leonardi, N. Donato, G. Neri, Effect of indium doping on ZnO based-gas sensor for CO, Mater. Sci. Semicond. Process. 27 (2014) 319–325, https://doi.org/10.1016/j.mssp.2014.07.009.

[6] X. Kuang, T. Liu, Y. Zhang, W. Wang, M. Yang, W. Zeng, S. Hussain, X. Peng, Urchin-like SnO2 nanoflowers via hydrothermal synthesis and their gas sensing properties, Mater. Lett. 161 (2015) 153–156, https://doi.org/10.1016/j.matlet.2015.08.090.

[7] U.T. Nakate, R. Ahmad, P. Patil, Y. Yu, Y.-B. Hahn, Ultra thin NiO nanosheets for high performance hydrogen gas sensor device, Appl. Surf. Sci. 506 (2020) 144971, https://doi.org/10.1016/j.apsusc.2019.144971.

[8] A. Yang, D. Wang, T. Lan, J. Chu, W. Li, J. Pan, Z. Liu, X. Wang, M. Rong, Single ultrathin WO3 nanowire as a superior gas sensor for SO2 and H2S: selective adsorption and distinct IV response, Mater. Chem. Phys. 240 (2020) 122165, https://doi.org/10.1016/j.matchemphys.2019.122165.

[9] P. Chakrabarty, M. Banik, N. Gogurla, S. Santra, S.K. Ray, R. Mukherjee, Light trapping-mediated room-temperature gas sensing by ordered ZnO nano structures decorated with plasmonic Au nanoparticles, ACS Omega 4 (2019) 12071–12080, https://doi.org/10.1021/acsomega.9b01116.

[10] X. Geng, D. Lahem, C. Zhang, C.-J. Li, M.-G. Olivier, M. Debliquy, Visible light enhanced black NiO sensors for ppb-level NO2 detection at room temperature, Ceram. Int. 45 (2019) 4253–4261, https://doi.org/10.1016/j.ceramint.2018.11.097.

[11] U.T. Nakate, P. Patil, B. Ghule, Y.T. Nakate, S. Ekar, R.C. Ambare, R. Mane, Room temperature LPG sensing properties using spray pyrolysis deposited nano-crystalline CdO thin films, Surf Interfaces 17 (2019) 100339, https://doi.org/10.1016/j.surfin.2019.100339.

[12] E. Fazio, M. Hjiri, R. Dhahri, L. El Mir, G. Sabatino, F. Barreca, F. Neri, S. Leonardi, A. Pistone, G. Neri, Ammonia sensing properties of V-doped ZnO: Ca nanopowders prepared by sol–gel synthesis, J. Solid State Chem. 226 (2015) 192–200, https://doi.org/10.1016/j.jssc.2015.02.021.

[13] M. Hjiri, L. El Mir, S. Leonardi, A. Pistone, L. Mavilia, G. Neri, Al-doped ZnO for highly sensitive CO gas sensors, Sens. Actuators, B 196 (2014) 413–420, https://doi.org/10.1016/j.snb.2014.01.068.

[14] M. Hjiri, R. Dhahri, L. El Mir, A. Bonavita, N. Donato, S. Leonardi, G. Neri, CO sensing properties of Ga-doped ZnO prepared by sol–gel route, J. Alloys Compd. 634 (2015) 187–192, https://doi.org/10.1016/j.jallcom.2015.02.083.

[15] R. Dhahri, S. Leonardi, M. Hjiri, L. El Mir, A. Bonavita, N. Donato, D. Iannazzo, G. Neri, Enhanced performance of novel calcium/aluminum co-doped zinc oxide for CO2 sensors, Sens. Actuators, B 239 (2017) 36–44, https://doi.org/10.1016/j.snb.2016.07.155.

[16] H. Qin, T. Liu, J. Liu, Q. Liu, R. Li, H. Zhang, J. Wang, Fabrication of uniform 1-D ZnO/ZnCo2O4 nano-composite and enhanced properties in gas sensing detection, Mater. Chem. Phys. 228 (2019) 66–74, https://doi.org/10.1016/j.matchemphys.2019.02.051.

[17] G. Srinet, R. Kumar, V. Sajal, Effects of aluminium doping on structural and photoluminescence properties of ZnO nanoparticles, Ceram. Int. 40 (2014) 4025–4031, https://doi.org/10.1016/j.ceramint.2013.08.055.

[18] H. Aydın, F. Yakuphanoglu, C. Aydın, Al-doped ZnO as a multifunctional nanomaterial: structural, morphological, optical and low-temperature gas sensing properties, J. Alloys Compd. 773 (2019) 802–811, https://doi.org/10.1016/j.jallcom.2018.09.327.

[19] K. Omri, I. Najeh, R. Dhahri, J. El Ghoul, L. El Mir, Effects of temperature on the optical and electrical properties of ZnO nanoparticles synthesized by sol–gel method, Microelectron. Eng. 128 (2014) 53–58, https://doi.org/10.1016/j.mee.2014.05.029.

[20] S. Nkosi, I. Kortidis, D. Motaung, R. Kroon, N. Leshabane, J. Tshilongo, O. Ndwandwe, The effect of stabilized ZnO nanostructures green luminescence towards LPG sensing capabilities, Mater. Chem. Phys. 242 (2020) 122452, https://doi.org/10.1016/j.matchemphys.2019.122452.

[21] K. Girija, K. Somasundaram, A. Debnath, A. Topkar, R. Vatsa, Enhanced H2S sensing properties of Gallium doped ZnO nanocrystalline films as investigated by DC conductivity and impedance spectroscopy, Mater. Chem. Phys. 214 (2018) 297–305, https://doi.org/10.1016/j.matchemphys.2018.04.104.

[22] S. Kanaparthi, S.G. Singh, Chemiresistive sensor based on zinc oxide nanoflakes for CO2 detection, Nanostruct. Mater. 2 (2019) 700–706, https://doi.org/10.1021/acsanm.8b01763.

[23] N. Zahmouli, M. Hjiri, L. El Mir, A. Bonavita, N. Donato, G. Neri, S.G. Leonardi, High performance acetone sensor based on γ-Fe2O3/Al–ZnO nanocomposites, Nanotechnology 30 (2018) 055502, https://doi.org/10.1088/1361-6528/aaf069.

[24] M. Hjiri, N. Zahmouli, R. Dhahri, S. Leonardi, L. El Mir, G. Neri, Doped-ZnO nanoparticles for selective gas sensors, J. Mater. Sci. Mater. Electron. 28 (2017) 9667–9674, https://doi.org/10.1007/s10854-017-6717-9.

[25] T.T.O. Nguyen, T.H. Truong, A.T. Le, T. Dai Nguyen, Facile synthesis of different ZnO nanostructures for detecting sub-ppm NO2 gas, Mater. Today Commun. 22 (2020) 100826, https://doi.org/10.1016/j.mtcomm.2019.100826.

[26] S. Kanaparthi, S.G. Singh, Highly sensitive and ultra-fast responsive ammonia gas sensor based on 2D ZnO nanoflakes, Mater. Sci. Energy Technol 3 (2020) 91–96, https://doi.org/10.1016/j.mset.2019.10.010.

[27] B. Zhang, Y. Wang, X. Meng, Z. Zhang, S. Mu, High response methane sensor based on Au-modified hierarchical porous nanosheets-assembled ZnO microspheres, Mater. Chem. Phys. (2020) 123027, https://doi.org/10.1016/j.matchemphys.2020.123027.

[28] S. Jaballah, M. Benamara, H. Dahman, D. Lahem, M. Debliquy, L. El Mir, Formaldehyde sensing characteristics of calcium-doped zinc oxide nanoparticles-based gas sensor, J. Mat. Sci. Mater. Electron. 31 (2020) 8230–8239, https://doi.org/10.1007/s10854-020-03358-y.

[29] M. Hjiri, R. Dhahri, K. Omri, L. El Mir, S. Leonardi, N. Donato, G. Neri, Effect of indium doping on ZnO based-gas sensor for CO, Mater. Sci. Semicond. Process. 27 (2014) 319–325, https://doi.org/10.1016/j.mssp.2014.07.009.

[30] A. Mahroug, B. Mari, M. Mollar, I. Boudjadar, L. Guerbous, A. Henni, N. Selmi, Studies on structural, surface morphological, optical, luminescence and Uv photodetection properties of sol–gel Mg-doped ZnO thin films, Surf. Rev. Lett. 26 (2019) 1850167, https://doi.org/10.1142/S0218625X18501676.

[31] V. Khorramshahi, J. Karamdel, R. Yousefi, Acetic acid sensing of Mg-doped ZnO thin films fabricated by the sol–gel method, J. Mater. Sci. Mater. Electron. 29 (2018) 14679–14688, https://doi.org/10.1007/s10854-018-9604-0.

[32] M. Amin, N.A. Shah, A.S. Bhatti, M.A. Malik, Effects of Mg doping on optical and CO gas sensing properties of sensitive ZnO nanobelts, CrystEngComm 16 (2014) 6080–6088, https://doi.org/10.1039/C4CE00153B.

[33] A.J. Kulandaisamy, J.R. Reddy, P. Srinivasan, K.J. Babu, G.K. Mani, P. Shankar, J. B.B. Rayappan, Room temperature ammonia sensing properties of ZnO thin films grown by spray pyrolysis: effect of Mg doping, J. Alloys Compd. 688 (2016) 422–429, https://doi.org/10.1016/j.jallcom.2016.07.050.

[34] R. Slama, J. El Ghoul, I. Ghiloufi, K. Omri, L. El Mir, A. Houas, Synthesis and physico-chemical studies of vanadium doped zinc oxide nanoparticles and its photocatalysis, Sci. Mater. Electron. 27 (2016) 8146–8153, https://doi.org/10.1007/s10854-016-4817-6.

[35] A. Mahmoud, M. Echabaane, K. Omri, L. El Mir, R.B. Chaabane, Development of an impedimetric non enzymatic sensor based on ZnO and Cu doped ZnO nanoparticles for the detection of glucose, J. Alloys Compd. 786 (2019) 960–968, https://doi.org/10.1016/j.jallcom.2019.02.060.

[36] I. Ghiloufi, J. El Ghoul, A.-E. Modwi, I. AlShunaifi, L. El Mir, Removal of lead (II) ion from aqueous solution using Ga-doped ZnO and Ca-doped ZnO nanopowder, Zeitschrift fur Naturforsch. Sect. A J. Phys. Sci. 74 (2019) 573–580, https://doi.org/10.1515/zna-2018-0443.

[37] I. Ghiloufi, J. El Ghoul, A. Modwi, L. El Mir, Preparation and characterization of Ca-doped zinc oxide nanoparticles for heavy metal removal from aqueous solution, MRS. Adv 1 (2016) 3607–3612, https://doi.org/10.1557/adv.2016.511.

[38] A. Alyamani, A. Tataroğlu, L. El Mir, A.A. Al-Ghamdi, H. Dahman, W. Farooq, F. Yakuphanoğlu, Photoresponse and photocapacitor properties of Au/AZO/p-Si/Al diode with AZO film prepared by pulsed laser deposition (PLD) method, Appl. Phys. A 122 (2016) 297, https://doi.org/10.1007/s00339-016-9812-5.

[39] S. Mourad, J. El Ghoul, K. Khirouni, Role of indium doping on structural and electrical properties of ZnO nanoparticles prepared by sol–gel method, Sci. Mater. Electron. (2020) 1–13, https://doi.org/10.1007/s10854-020-03193-1.

[40] H. Gao, L. Xie, P. Gong, H. Wang, Detection of ethanol using a tunable interband cascade laser at 3.345 μm, Photonic Sens 8 (2018) 303–309, https://doi.org/10.1007/s13320-018-0471-3.

[41] N. Jayababu, M. Poloju, J. Shruthi, M.R. Reddy, Semi shield driven pn heterostructures and their role in enhancing the room temperature ethanol gas sensing performance of NiO/SnO2 nanocomposites, Ceram. Int. 45 (2019) 15134–15142, https://doi.org/10.1016/j.ceramint.2019.04.255.

[42] S. Jongen, A. Vermeeren, N. van der Sluiszen, M.B. Schumacher, E. Theunissen, K. Kuypers, E. Vuurman, J. Ramaekers, A pooled analysis of on-the-road highway driving studies in actual traffic measuring standard deviation of lateral position (ie, "weaving") while driving at a blood alcohol concentration of 0.5 g/L, Psychopharmacology 234 (2017) 837–844, https://doi.org/10.1007/s00213-016-4519-z.

[43] L. Li, C. Zhang, R. Zhang, X. Gao, S. He, M. Liu, X. Li, W. Chen, 2D ultrathin Co3O4 nanosheet array deposited on 3D carbon foam for enhanced ethanol gas sensing application, Sens. Actuators, B 244 (2017) 664–672, https://doi.org/10.1016/j.snb.2017.01.056.

[44] C. Sun, S. Rajasekhara, Y. Chen, J.B. Goodenough, Facile synthesis of monodisperse porous Co 3 O 4 microspheres with superior ethanol sensing properties, ChemComm 47 (2011) 12852–12854, https://doi.org/10.1039/C1CC15555E.

[45] T. Arakawa, T. Suzuki, M. Tsujii, K. Iitani, P.-J. Chien, M. Ye, K. Toma, Y. Iwasaki, K. Mitsubayashi, Real-time monitoring of skin ethanol gas by a high-sensitivity gas phase biosensor (bio-sniffer) for the non-invasive evaluation of volatile blood compounds, Biosens. Bioelectron. 129 (2019) 245–253, https://doi.org/10.1016/j.bios.2018.09.070.

[46] J. Liu, T. Wang, B. Wang, P. Sun, Q. Yang, X. Liang, H. Song, G. Lu, Highly sensitive and low detection limit of ethanol gas sensor based on hollow ZnO/SnO2 spheres composite material, Sens. Actuators, B 245 (2017) 551–559, https://doi.org/10.1016/j.snb.2017.01.148.

[47] M. GuI, M. Amin, M. Abbas, S.Z. Ilyas, N.A. Shah, Synthesis and characterization of magnesium doped ZnO nanostructures: methane (CH 4) detection, Sci. Mater. Electron. 30 (2019) 5257–5265, https://doi.org/10.1007/s10854-019-00825-z.

[48] K. Vijayalakshmi, K. Karthick, Growth of highly c-axis oriented Mg: ZnO nanorods on Al2O3 substrate towards high-performance H2 sensing, Int. J. Hydrogen Energy 39 (2014) 7165–7172, https://doi.org/10.1016/j.ijhydene.2014.02.123.

[49] C.-H. Kwak, H.-S. Woo, F. Abdel-Hady, A. Wazzan, J.-H. Lee, Vapor-phase growth of urchin-like Mg-doped ZnO nanowire networks and their application to highly sensitive and selective detection of ethanol, Sens. Actuators, B 223 (2016) 527–534, https://doi.org/10.1016/j.snb.2015.09.120.

[50] L. El Mir, Z.B. Ayadi, M. Saadoun, K. Djessas, H.J. von Bardeleben, S. Alaya, Preparation and characterization of n-type conductive (Al, Co) co-doped ZnO thin films deposited by sputtering from aerogel nanopowders, Appl. Surf. Sci. 254 (2007) 570–573, https://doi.org/10.1016/j.apsusc.2007.06.028.

[51] L. El Mir, J. El Ghoul, S. Alaya, M.B. Salem, C. Barthou, H. Von Bardeleben, Synthesis and luminescence properties of vanadium-doped nanosized zinc oxide aerogel, Phys. B Condens. Matter 403 (2008) 1770–1774, https://doi.org/10.1016/j.physb.2007.10.069.

[52] C. Zhang, A. Boudiba, C. Navio, C. Bittencourt, M.-G. Olivier, R. Snyders, M. Debliquy, Highly sensitive hydrogen sensors based on co-sputtered platinum-activated tungsten oxide films, Int. J. Hydrogen Energy 36 (2011) 1107–1114, https://doi.org/10.1016/j.ijhydene.2010.10.011.

[53] X. Geng, J. You, C. Zhang, Microstructure and sensing properties of CdS-ZnO1− x coatings deposited by liquid plasma spray and treated with hydrogen peroxide solution for nitrogen dioxide detection at room temperature, J. Alloys Compd. 687 (2016) 286–293, https://doi.org/10.1016/j.jallcom.2016.06.079.

[54] C. Zhang, X. Geng, H. Liao, C.-J. Li, M. Debliquy, Room-temperature nitrogen-dioxide sensors based on ZnO1− x coatings deposited by solution precursor plasma spray, Sens. Actuators, B 242 (2017) 102–111, https://doi.org/10.1016/j.snb.2016.11.024.

[55] X. Geng, C. Zhang, Y. Luo, M. Debliquy, Preparation and characterization of CuxO1-y@ ZnO1-α nanocomposites for enhanced room-temperature NO2 sensing applications, Appl. Surf. Sci. 401 (2017) 248–255, https://doi.org/10.1016/j.apsusc.2017.01.014.

[56] S. Muthukumaran, R. Gopalakrishnan, Structural, FTIR and photoluminescence studies of Cu doped ZnO nanopowders by co-precipitation method, Opt. Mater. 34 (2012) 1946–1953, https://doi.org/10.1016/j.optmat.2012.06.004.

[57] M. El-Hilo, A. Dakhel, Structural and magnetic properties of Mn-doped ZnO powders, J. Magn. Magn Mater. 323 (2011) 2202–2205, https://doi.org/10.1016/j.jmmm.2011.03.031.

[58] A. Kalita, M.P. Kalita, Microstructural, optical, magnetic and photocatalytic properties of Mn doped ZnO nanocrystals of different sizes, Phys. B Condens. Matter 552 (2019) 30–46, https://doi.org/10.1016/j.physb.2018.08.028.

[59] V. Mote, Y. Purushotham, B. Dole, Williamson-Hall analysis in estimation of lattice strain in nanometer-sized ZnO particles, J Theor Appl Phys 6 (2012) 6, https://doi.org/10.1186/2251-7235-6-6.

[60] M. Rouchdi, E. Salmani, B. Fares, N. Hassanain, A. Mzerd, Synthesis and characteristics of Mg doped ZnO thin films: experimental and ab-initio study, Results Phys 7 (2017) 620–627, https://doi.org/10.1016/j.rinp.2017.01.023.

[61] J. Yang, Y. Wang, J. Kong, M. Yu, H. Jin, Synthesis of Mg-doped hierarchical ZnO nanostructures via hydrothermal method and their optical properties, J. Alloys Compd. 657 (2016) 261–267, https://doi.org/10.1016/j.jallcom.2015.10.117.

[62] X. Liu, J. Zhang, L. Wang, T. Yang, X. Guo, S. Wu, S. Wang, 3D hierarchically porous ZnO structures and their functionalization by Au nanoparticles for gas sensors, J. Mater. Chem. 21 (2011) 349–356, https://doi.org/10.1039/C0JM01800G.

[63] A.L. Zou, Y. Qiu, J.J. Yu, B. Yin, G.Y. Cao, H.Q. Zhang, L.Z. Hu, Ethanol sensing with Au-modified ZnO microwires, Sens. Actuators, B 227 (2016) 65–72, https://doi.org/10.1016/j.snb.2015.12.023.

[64] M. Sudha, S. Radha, S. Kirubaveni, R. Kiruthika, R. Govindaraj, N. Santhosh, Experimental study on structural, optoelectronic and room temperature sensing performance of Nickel doped ZnO based ethanol sensors, Solid State Sci. 78 (2018) 30–39, https://doi.org/10.1016/j.solidstatesciences.2018.02.001.

[65] N.S. Ramgir, M. Kaur, P.K. Sharma, N. Datta, S. Kailasaganapathi, S. Bhattacharya, A.K. Debnath, D.K. Aswal, S.K. Gupta, Ethanol sensing properties of pure and Au modified ZnO nanowires, Sens. Actuators, B l 187 (2013) 313–318, https://doi.org/10.1016/j.snb.2013.01.079.

[66] J. Sun, S. Bai, Y. Tian, Y. Zhao, N. Han, R. Luo, D. Li, A. Chen, Hybridization of ZnSnO3 and rGO for improvement of formaldehyde sensing properties, Sens. Actuators, B 257 (2018) 29–36, https://doi.org/10.1016/j.snb.2017.10.015.

[67] J. Law, J. Thong, Improving the NH3 gas sensitivity of ZnO nanowire sensors by reducing the carrier concentration, Nanotechnology 19 (2008) 205502, https://doi.org/10.1088/0957-4484/19/20/205502.

[68] M. Bagheri, A.A. Khodadadi, A.R. Mahjoub, Y. Mortazavi, Gallia–ZnO nanohybrid sensors with dramatically higher sensitivity to ethanol in presence of CO, methane and VOCs, Sens. Actuators, B 223 (2016) 576–585, https://doi.org/10.1016/j.snb.2015.09.137.

[69] F. Cao, C. Li, M. Li, H. Li, X. Huang, B. Yang, Direct growth of Al-doped ZnO ultrathin nanosheets on electrode for ethanol gas sensor application, Appl. Surf. Sci. 447 (2018) 173–181, https://doi.org/10.1016/j.apsusc.2018.03.217.

[70] Y. Wei, X. Wang, G. Yi, L. Zhou, J. Cao, G. Sun, Z. Chen, H. Bala, Z. Zhang, Hydrothermal synthesis of Ag modified ZnO nanorods and their enhanced ethanol-sensing properties, Mater. Sci. Semicond. Process. 75 (2018) 327–333, https://doi.org/10.1016/j.mssp.2017.11.007.

[71] Y. Zhang, Y. Liu, L. Zhou, D. Liu, F. Liu, F. Liu, X. Liang, X. Yan, Y. Gao, G. Lu, The role of Ce doping in enhancing sensing performance of ZnO-based gas sensor by adjusting the proportion of oxygen species, Sens. Actuators, B 273 (2018) 991–998, https://doi.org/10.1016/j.snb.2018.05.167.

[72] A. Sáaedi, R. Yousefi, Improvement of gas-sensing performance of ZnO nanorods by group-I elements doping, Int. J. Appl. Phys. 122 (2017) 224505, https://doi.org/10.1063/1.5009249.

[73] J. Xu, S. Li, L. Li, L. Chen, Y. Zhu, Facile fabrication and superior gas sensing properties of spongelike Co-doped ZnO microspheres for ethanol sensors, Ceram. Int. 44 (2018) 16773–16780, https://doi.org/10.1016/j.ceramint.2018.06.110.